

# Quantum WDM fermions and gravitation determine the observed galaxy structures

C. Destri <sup>(a),\*</sup> H. J. de Vega <sup>(b,c),†</sup> and N. G. Sanchez <sup>(c)‡</sup>

<sup>(a)</sup> *Dipartimento di Fisica G. Occhialini, Università Milano-Bicocca and INFN, sezione di Milano-Bicocca, Piazza della Scienza 3, 20126 Milano, Italia.*

<sup>(b)</sup> *LPTHE, Université Pierre et Marie Curie (Paris VI), Laboratoire Associé au CNRS UMR 7589, Tour 13, 4ème. et 5ème. étages, Boite 126, 4, Place Jussieu, 75252 Paris, Cedex 05, France.*

<sup>(c)</sup> *Observatoire de Paris, LERMA. Laboratoire Associé au CNRS UMR 8112. 61, Avenue de l'Observatoire, 75014 Paris, France.*

(Dated: January 14, 2013)

Quantum mechanics is necessary to compute galaxy structures at kpc scales and below. This is so because near the galaxy center, at scales below  $10 - 100$  pc, warm dark matter (WDM) **quantum** effects are important: observations show that the interparticle distance is of the order of, or smaller than the de Broglie wavelength for WDM. This explains why all classical (non-quantum) WDM  $N$ -body simulations fail to explain galactic cores and their sizes. We describe fermionic WDM galaxies in an analytic semiclassical framework based on the Thomas-Fermi approach, we resolve it numerically and find the main physical galaxy magnitudes: mass, halo radius, phase-space density, velocity dispersion, fully consistent with observations, including compact dwarf galaxies. Namely, fermionic WDM treated quantum mechanically, as it must be, reproduces the observed galaxy DM cores and their sizes. [In addition, as is known, WDM simulations produce the right DM structures in agreement with observations for scales  $\gtrsim$  kpc]. We show that compact dwarf galaxies are natural quantum macroscopic objects supported against gravity by the fermionic WDM quantum pressure (quantum degenerate fermions) with a **minimal** galaxy mass and **minimal** velocity dispersion. Interestingly enough, the minimal galaxy mass implies a minimal mass  $m_{min}$  for the WDM particle. The lightest known dwarf galaxy (Willman I) implies  $m > m_{min} = 1.91$  keV. These results and the observed halo radius and mass of the compact galaxies provide further indication that the WDM particle mass  $m$  is approximately around 2 keV.

PACS numbers: 95.35.+d, 98.52.-b, 98.56.Wm, 98.62.Gq

## Contents

<b>I. Introduction and summary of results</b>	1
A. Dwarf galaxies as WDM quantum macroscopic objects	5
B. Dwarf Galaxies supported by WDM fermionic quantum pressure	5
<b>II. General Galaxy properties from quantum fermionic WDM in the Thomas-Fermi approach</b>	6
A. Quantum degenerate limit: compact dwarf galaxies and minimal galaxy mass	9
B. Classical dilute limit: large galaxies	11
C. Physical galaxy properties from compact dwarf galaxies to large galaxies	11
<b>Acknowledgments</b>	14
<b>References</b>	14

## I. INTRODUCTION AND SUMMARY OF RESULTS

Dark matter (DM) is the main component of galaxies, especially of dwarf galaxies which are almost exclusively formed by DM. It thus appears that the study of galaxy properties is an excellent way to disentangle the nature of DM.

---

\*Electronic address: Claudio.Destri@mib.infn.it

†Electronic address: devega@lpthe.jussieu.fr

‡Electronic address: Norma.Sanchez@obspm.fr

Cold DM (CDM) produces an overabundance of substructures below the  $\sim 50$  kpc till very small scales  $\sim 0.005$  pc which constitutes, as is well known, one of the most serious drawbacks for CDM. On the contrary, warm DM (WDM), that is, DM particles with mass in the keV scale, produces DM structures in the range of scales  $\lesssim 50$  kpc in agreement with observations. In WDM structure formation, substructures below the free-streaming scale  $\sim 50$  kpc are not formed, contrary to the case of CDM. This conclusion for WDM based on the linear theory is robustly confirmed by  $N$ -body simulations by different groups [1]. For scales larger than  $\sim 50$  kpc, WDM yields the same results than CDM and agrees with all the observations: small scale as well as large scale structure observations and CMB anisotropy observations.

Astronomical observations show that the DM galaxy density profiles are **cored** till scales below the kpc [2–4]. On the other hand,  $N$ -body CDM simulations exhibit cusped density profiles with a typical  $1/r$  behaviour near the galaxy center  $r = 0$ . Classical  $N$ -body WDM simulations exhibit cusps or small cores smaller than the observed cores [6, 15].

Numerical calculations based on the spherically symmetric Vlasov–Poisson equation from the Larson moment expansion [7], as well as on the exact dynamics of the associated  $N$ -body system, have confirmed these findings [8].

A direct way to see whether a system of particles has a classical or quantum nature is to compare the particle de Broglie wavelength  $\lambda_{dB}$  with the inter-particle distance  $d$ . We investigate this issue in sec. I A and express the ratio of the two lengths as

$$\mathcal{R} \equiv \frac{\lambda_{dB}}{d} = \hbar \left( \frac{Q_h}{m^4} \right)^{\frac{1}{3}} \quad , \quad Q_h \equiv \frac{\rho_h}{\sigma^3} .$$

where  $Q_h$  is the DM phase space density,  $\rho_h$  and  $\sigma$  being the halo density and the velocity dispersion, respectively. Values of  $\mathcal{R}$  much smaller than unity correspond to classical physics while  $\mathcal{R} \sim 1$  or larger corresponds to the quantum regime. The observed values of  $Q_h$  from Table I yields  $\mathcal{R}$  in the range

$$2 \times 10^{-3} < \mathcal{R} \left( \frac{m}{\text{keV}} \right)^{\frac{4}{3}} < 1.4 . \quad (1.1)$$

The larger value of  $\mathcal{R}$  is for ultracompact dwarf galaxies and the smaller value of  $\mathcal{R}$  is for large spirals. The values of  $\mathcal{R}$  around unity clearly imply (and solely from observations) that compact dwarf galaxies are natural *macroscopic quantum objects* for WDM.

WDM fermions always provide a non-zero pressure of quantum nature. By balancing this quantum pressure with the gravitation pressure, we find theoretical values for the total mass  $M \sim 10^6 M_\odot$ , the radius  $R \sim 30$  pc and the velocity dispersion  $\sigma \sim 2$  km/s which are consistent with the observations of compact dwarf galaxies (see Table I). These results back the idea that dwarf galaxies are supported by the fermionic *WDM quantum pressure*.

Classical  $N$ -body simulations for DM are not valid at scales where the interparticle distance becomes of the order of, or smaller than, the de Broglie wavelength. This precisely happens near the galaxy center for WDM particles with mass  $m \sim \text{keV}$ . Therefore, the results of classical (non-quantum) WDM  $N$ -body simulations at such scales are not valid. This explains why all classical WDM  $N$ -body simulations fail to correctly reproduce the observed galaxy cores [15]. Classical  $N$ -body simulations are reliable for CDM because the mass of the CDM particle is large enough ( $m \sim \text{GeV}$ ) and then  $\mathcal{R} \ll 1$ . Such reliable CDM simulations always produce cusped galaxy profiles in contradiction with the observations.

Richard P. Feynman foresaw the necessity to include quantum physics in simulations [5]:

*“I’m not happy with all the analyses that go with just the classical theory, because nature isn’t classical, dammit, and if you want to make a simulation of nature, you’d better make it quantum mechanical, and by golly it’s a wonderful problem, because it doesn’t look so easy.”*

We treat here the self-gravitating fermionic DM in the Thomas-Fermi approximation. In this approach, the DM chemical potential  $\mu(r) = \mu_0 - m \phi(r)$ , where  $\mu_0$  is a constant and  $\phi(r)$  the gravitational potential, obeys the selfconsistent Poisson equation

$$\frac{d^2\mu}{dr^2} + \frac{2}{r} \frac{d\mu}{dr} = -\frac{4\pi G m^2}{\pi^2 \hbar^3} \int_0^\infty p^2 dp f(e(p) - \mu(r)) \quad (1.2)$$

where  $G$  is Newton’s gravitational constant,  $p$  is the DM particle momentum,  $e(p) = p^2/(2m)$  is the DM particle kinetic energy and  $f(E)$  is the energy distribution function. This is a semiclassical gravitational approach to determine selfconsistently the gravitational potential of the fermionic WDM given its distribution function  $f$ .

The boundary condition  $\mu'(0) = 0$  at the origin guarantees bounded central DM mass densities.

The distribution function  $f(E)$  (or a more general form with a dependence on other constants of the motion besides  $E$ ) is determined by the DM evolution since decoupling. Such quantum dynamical calculation is beyond the scope of the present paper.  $f(E)$  can be modeled for instance by the equilibrium Fermi-Dirac distributions or by out of equilibrium distributions. The galaxy magnitudes turn to be rather insensible to whether one chooses equilibrium or out of equilibrium distributions  $f(E)$  [9].

We get a one parameter family of solutions of eqs.(1.2) parametrized by the value of the chemical potential at the origin  $\mu(0)$  that can be expressed in terms of the phase-space density at the origin  $Q(0)$ . Large positive values of  $\mu(0)$  correspond to most compact object (fermions in the quantum degenerate limit), while large negative values of  $\mu(0)$  yield dilute objects (classical limit).

We show that the Thomas-Fermi equation implies the local equation of state

$$P(r) = \sigma^2(r) \rho(r) \quad \text{and the hydrostatic equilibrium equation} \quad \frac{dP}{dr} + \rho(r) \frac{d\phi}{dr} = 0 .$$

This local equation of state generalizes the local perfect fluid equation for  $r$ -dependent velocity  $v(r)$ .

The numerical resolution of eqs.(1.2) for the whole range of the chemical potential at the origin  $\mu(0)$  yields the physical galaxy magnitudes, such as mass, halo radius, phase-space density and velocity dispersion all fully compatible with observations including compact dwarf galaxies as can be seen from figs. 1 and 2 and Table I.

Approaching the classical diluted limit yields larger and larger halo radii, galaxy masses and velocity dispersions. Their maximum values are limited by the initial conditions provided by the primordial power spectrum which determines the sizes and masses of the galaxies formed. The phase space density decreases from its maximum value for the compact dwarf galaxies corresponding to the degenerate fermions limit till its smallest value for large galaxies (spirals and ellipticals) corresponding to the classical dilute regime. The theoretical values for the core radius  $r_h$ , the core galaxy mass  $M_h$  and the velocity dispersion  $\sigma(0)$  obtained in the Thomas-Fermi framework vary very little with the specific form of the distribution function  $f(E)$ .

We display in fig. 1 the density and velocity profiles,  $\rho(r)/\rho(0)$  and  $\sigma(r)/\sigma(0)$  obtained in the Thomas-Fermi approach for different values of the chemical potential at the origin  $\mu(0)$ . Large positive values of  $\mu(0)$  correspond to the compact galaxies, while negative values of  $\mu(0)$  correspond to the classical regime describing spiral and elliptical galaxies. All density profiles are cored. The sizes of the cores  $r_h$  are in agreement with the observations, from the compact galaxies where  $r_h \sim 35$  pc till the spiral and elliptical galaxies where  $r_h \sim 0.2 - 60$  kpc. The larger and positive is  $\mu(0)$ , the smaller is the core. The minimal one arises in the degenerate case  $\mu(0) \rightarrow +\infty$  (compact dwarf galaxies).

In the left panel of fig. 2, we plot the (dimensionless) galaxy phase-space density  $\hbar^3 Q(0)/(\text{keV})^4$  obtained from the numerical resolution of the Thomas-Fermi eqs.(1.2) for WDM fermions of mass  $m = 1$  and 2 keV. The observed values of  $\hbar^3 Q_h/(\text{keV})^4$  and  $r_h$  from Table I are also depicted. The theoretical Thomas-Fermi curves in fig. 2 appear slightly below the observational data in all the range of galaxies most likely because the observed values  $Q_h$  (derived from the stars' velocity dispersion) are in fact upper bounds for the DM  $Q_h$ .

In the right panel of fig. 2, we plot the galaxy masses  $(M_h/M_\odot)\sqrt{M_\odot/\text{pc}^3} \rho_0$  obtained from the numerical resolution of the Thomas-Fermi eqs.(1.2), where  $M_h$  is the mass inside the halo radius and  $\rho_0$  the observed central mass density. We observe a good agreement between the Thomas-Fermi results and the observations in **all** the range of galaxies for a DM particle mass  $m$  around 2 keV. Notice that the error bars of the observational data are not reported here but they are at least about 10 – 20%.

For degenerate fermions [ $\mu(0) \rightarrow +\infty$ ] the halo radius, the velocity dispersion and the galaxy mass take their *minimum* values. These minimum values eqs.(2.25) and (2.25) obtained in the Thomas-Fermi approach are similar to the estimates provided in sec. IB through a simple balancing argument between the gravitational and quantum pressures.

The masses of compact dwarf galaxies dominated by DM must be larger than this minimum mass  $M_{h,min}$ . The lightest known galaxy of this kind is Willman I (see Table I). Imposing  $M_{h,min} < M_{\text{Willman I}} = 2.9 \cdot 10^4 M_\odot$  provides a minimal mass (a lower bound) for the WDM particle:

$$m > m_{min} = 1.91 \text{ keV} . \quad (1.3)$$

This minimal WDM mass is *independent* of the WDM particle physics model.  $m_{min}$  is an **universal** value irrespective of the shape of the distribution function  $f(E)$  in the non-degenerate regime.

Galaxy	$r_h$ pc	$\frac{\sigma}{\frac{\text{km}}{\text{s}}}$	$\frac{\hbar^{\frac{3}{2}} \sqrt{Q_h}}{(\text{keV})^2}$	$\rho(0)/\frac{M_\odot}{(\text{pc})^3}$	$\frac{M_h}{10^6 M_\odot}$
Willman 1	19	4	0.85	6.3	0.029
Segue 1	48	4	1.3	2.5	1.93
Leo IV	400	3.3	0.2	.19	200
Canis Venatici II	245	4.6	0.2	0.49	4.8
Coma-Berenices	123	4.6	0.42	2.09	0.14
Leo II	320	6.6	0.093	0.34	36.6
Leo T	170	7.8	0.12	0.79	12.9
Hercules	387	5.1	0.078	0.1	25.1
Carina	424	6.4	0.075	0.15	32.2
Ursa Major I	504	7.6	0.066	0.25	33.2
Draco	305	10.1	0.06	0.5	26.5
Leo I	518	9	0.048	0.22	96
Sculptor	480	9	0.05	0.25	78.8
Boötes I	362	9	0.058	0.38	43.2
Canis Venatici I	1220	7.6	0.037	0.08	344
Sextans	1290	7.1	0.021	0.02	116
Ursa Minor	750	11.5	0.028	0.16	193
Fornax	1730	10.7	0.016	0.053	1750
NGC 185	450	31	0.033	4.09	975
NGC 855	1063	58	0.01	2.64	8340
Small Spiral	5100	40.7	0.0018	0.029	6900
NGC 4478	1890	147	0.003	3.7	$6.55 \times 10^4$
Medium Spiral	$1.9 \times 10^4$	76.2	$3.7 \times 10^{-4}$	0.0076	$1.01 \times 10^5$
NGC 731	6160	163	$9.27 \times 10^{-4}$	0.47	$2.87 \times 10^5$
NGC 3853	5220	198	$8.8 \times 10^{-4}$	0.77	$2.87 \times 10^5$
NGC 499	7700	274	$5.9 \times 10^{-4}$	0.91	$1.09 \times 10^6$
Large Spiral	$5.9 \times 10^4$	125	$0.96 \times 10^{-4}$	$2.3 \times 10^{-3}$	$1. \times 10^6$

TABLE I: Observed values  $r_h$ ,  $\sigma$ ,  $\sqrt{Q_h}$ ,  $\rho(0)$  and  $M_h$  covering from ultracompact galaxies to large spiral galaxies from refs.[3, 4, 11, 12, 16–20]. The phase space density is larger for smaller galaxies, both in mass and size. Notice that the phase space density is obtained from the stars velocity dispersion which is expected to be smaller than the DM velocity dispersion. Therefore, the reported  $Q_h$  are in fact upper bounds to the true values [16].

Interestingly enough, comparison of the theoretically derived galaxy masses with the galaxy data plotted in fig. 2 indicates a WDM particle mass  $m$  approximately around 2 keV in agreement with earlier estimations [10, 12]. If the WDM particle mass would be  $m \gg 1$  keV, an overabundance of small galaxies (small scale structures) without observable counterpart would appear.

In summary, the theoretical Thomas-Fermi results are fully consistent with all the observations including dwarf compact galaxies as can be seen from figs. 1 and 2. It is highly remarkable that in the context of fermionic WDM the simple stationary quantum description provided by this semiclassical framework is able to reproduce such broad variety of galaxies.

These results indicate that fermionic WDM treated quantum mechanically (even approximately) is fully consistent with the observed galaxy properties including the DM core sizes. That is, quantum physics and the associated quantum pressure, **rule out** galaxy cusps for fermionic WDM and provide the right sized observed cores.

We have not considered baryons in the present analysis of the galaxies. This is fully justified for dwarf compact galaxies which are composed today 99.99% of dark matter [19, 21, 22]. In large galaxies the baryon fraction can reach values up to 1 - 3 % [14]. We have also ignored supermassive central black holes which appear in large spiral galaxies. In any case, it must be noticed that the central black hole mass is at most  $\sim 10^{-3}$  of the mass of the bulge.

Fermionic WDM by itself produce galaxies and structures in agreement with observations. Therefore, the effect of including baryons is expected to be a correction to the pure WDM results, consistent with the fact that dark matter is in average six times more abundant than baryons.

We use units such that the speed of light is  $c = 1$  throughout this paper.

### A. Dwarf galaxies as WDM quantum macroscopic objects

In order to determine whether a system of particles has a classical or quantum nature we should compare the particle de Broglie wavelength with the interparticle distance.

The de Broglie wavelength of DM particles in a galaxy can be expressed as

$$\lambda_{dB} = \frac{\hbar}{m \sigma}, \quad (1.4)$$

where  $\sigma$  is the velocity dispersion, while the average interparticle distance  $d$  can be estimated as

$$d = \left( \frac{m}{\rho_h} \right)^{\frac{1}{3}}, \quad (1.5)$$

where  $\rho_h$  is the average density in the galaxy core. We can measure the classical or quantum character of the system by considering the ratio

$$\mathcal{R} \equiv \frac{\lambda_{dB}}{d}$$

By using the phase-space density

$$Q_h \equiv \frac{\rho_h}{\sigma^3}$$

and eqs.(1.4)-(1.5),  $\mathcal{R}$  can be expressed as

$$\mathcal{R} = \hbar \left( \frac{Q_h}{m^4} \right)^{\frac{1}{3}}. \quad (1.6)$$

Notice that  $\mathcal{R}$  as well as  $Q_h$  are invariant under the expansion of the universe because both  $\lambda_{dB}$  and  $d$  scale with the expansion scale factor.  $\mathcal{R}$  and  $Q_h$  evolve by nonlinear gravitational relaxation.

Using now the observed values of  $Q_h$  from Table I yields  $\mathcal{R}$  in the range

$$2 \times 10^{-3} < \mathcal{R} \left( \frac{m}{\text{keV}} \right)^{\frac{4}{3}} < 1.4 \quad (1.7)$$

The larger value of  $\mathcal{R}$  is for ultracompact dwarfs while the smaller value of  $\mathcal{R}$  is for big spirals.

The ratio  $\mathcal{R}$  around unity clearly implies a macroscopic quantum object. Notice that  $\mathcal{R}$  expresses solely in terms of  $Q$  and hence  $(\hbar^3 Q/m^4)$  measures how quantum or classical is the system, here, the galaxy. Therefore, we conclude **solely from observations** that compact dwarf galaxies are natural macroscopic quantum objects for WDM.

### B. Dwarf Galaxies supported by WDM fermionic quantum pressure

For an order-of-magnitude estimate, let us consider a halo of mass  $M$  and radius  $R$  of fermionic matter. Each fermion can be considered inside a cell of size  $\Delta x \sim 1/n^{\frac{1}{3}}$  and therefore has a momentum

$$p \sim \frac{\hbar}{\Delta x} \sim \hbar n^{\frac{1}{3}}.$$

The associated quantum pressure  $P_q$  (flux of the momentum) has the value

$$P_q = n \sigma p \sim \hbar \sigma n^{\frac{4}{3}} = \frac{\hbar^2}{m} n^{\frac{5}{3}}. \quad (1.8)$$

where  $\sigma$  is the mean velocity given by

$$\sigma = \frac{p}{m} = \frac{\hbar}{m} n^{\frac{1}{3}}.$$

We estimate the number density as

$$n = \frac{M}{\frac{4}{3}\pi R^3 m},$$

and we use that  $p = m \sigma$  to obtain from eq.(1.8)

$$P_q = \frac{\hbar^2}{m R^5} \left( \frac{3 M}{4 \pi m} \right)^{\frac{5}{3}}. \quad (1.9)$$

On the other hand, as is well known, galaxy formation as all structure formation in the Universe is driven by gravitational physics. The system will be in dynamical equilibrium if this quantum pressure is balanced by the gravitational pressure

$$P_G = \text{gravitational force/area} = \frac{G M^2}{R^2} \times \frac{1}{4 \pi R^2} \quad (1.10)$$

Equating  $P_q = P_G$  from eqs.(1.10)-(1.9) yields the following expressions for the size  $R$  and the velocity  $\sigma$  in terms of the mass  $M$  of the system and the mass  $m$  of the particles,:

$$R = \frac{3^{\frac{5}{3}}}{(4 \pi)^{\frac{2}{3}}} \frac{\hbar^2}{G m^{\frac{8}{3}} M^{\frac{1}{3}}} = 10.61 \dots \text{pc} \left( \frac{10^6 M_{\odot}}{M} \right)^{\frac{1}{3}} \left( \frac{\text{keV}}{m} \right)^{\frac{8}{3}}, \quad (1.11)$$

$$\sigma = \left( \frac{4 \pi}{81} \right)^{\frac{1}{3}} \frac{G}{\hbar} m^{\frac{4}{3}} M^{\frac{2}{3}} = 11.62 \dots \frac{\text{km}}{\text{s}} \left( \frac{m}{\text{keV}} \right)^{\frac{4}{3}} \left( \frac{M}{10^6 M_{\odot}} \right)^{\frac{2}{3}}. \quad (1.12)$$

Notice that the values of  $M$ ,  $R$  and  $\sigma$  are consistent with the observed values of dwarf galaxies. Namely, for  $M$  of the order  $10^6 M_{\odot}$  (which is a typical mass value for dwarf galaxies),  $R$  and  $\sigma$  give the correct order of magnitude for the size and velocity dispersion of dwarf galaxies (see Table I) for a WDM particles mass in the keV scale.

These results back the idea that dwarf galaxies are supported by the fermionic *WDM quantum pressure* eq.(1.9).

It is useful to express the above quantities in terms of the density  $\rho$ , as follows

$$M = \frac{9 \hbar^3}{2 m^4} \sqrt{\frac{\rho}{\pi G^3}} = 0.7075 \dots 10^5 M_{\odot} \sqrt{\rho \frac{\text{pc}^3}{M_{\odot}}} \left( \frac{\text{keV}}{m} \right)^4, \quad R = \frac{3 \hbar}{2 \sqrt{\pi G}} \frac{1}{m^{\frac{4}{3}} \rho^{\frac{1}{6}}} = 25.66 \dots \text{pc} \left( \frac{M_{\odot}}{\rho \text{pc}^3} \right)^{\frac{1}{6}} \left( \frac{\text{keV}}{m} \right)^{\frac{4}{3}},$$

$$\sigma = \hbar \left( \frac{\rho}{m^4} \right)^{\frac{1}{3}} = 1.988 \dots \frac{\text{km}}{\text{s}} \left( \rho \frac{\text{pc}^3}{M_{\odot}} \right)^{\frac{1}{3}} \left( \frac{\text{keV}}{m} \right)^{\frac{4}{3}}, \quad P_q = \hbar^2 \frac{\rho^{\frac{5}{3}}}{m^{\frac{8}{3}}} = 0.04399 \dots \frac{M_{\odot}}{\text{kpc}^3} \left( \rho \frac{\text{pc}^3}{M_{\odot}} \right)^{\frac{5}{3}} \left( \frac{\text{keV}}{m} \right)^{\frac{8}{3}}. \quad (1.13)$$

$R$  and  $M$  are typical *semiclassical gravitational* quantities involving both  $G$  and  $\hbar$ . The particle velocity  $\sigma$  and the pressure  $P_q$  are of purely quantum mechanical origin.

## II. GENERAL GALAXY PROPERTIES FROM QUANTUM FERMIONIC WDM IN THE THOMAS-FERMI APPROACH

We consider a single DM halo in the late stages of structure formation when DM particles composing it are non-relativistic and their phase-space distribution function  $f(t, \mathbf{r}, \mathbf{p})$  is relaxing to a time-independent form, at least for  $\mathbf{r}$  not too far from the halo center. In the Thomas-Fermi approach such a time-independent form is taken to be a energy distribution function  $f(E)$  of the conserved single-particle energy  $E = p^2/(2m) - \mu$ , where  $m$  is the mass of the DM particle and  $\mu$  is the chemical potential

$$\mu(\mathbf{r}) = \mu_0 - m \phi(\mathbf{r}) \quad (2.1)$$

with  $\phi(\mathbf{r})$  the gravitational potential and  $\mu_0$  some constant.

We consider the spherical symmetric case where the Poisson equation for  $\phi(r)$  takes the form

$$\frac{d^2\mu}{dr^2} + \frac{2}{r} \frac{d\mu}{dr} = -4\pi G m \rho(r) , \quad (2.2)$$

where  $G$  is Newton's constant and  $\rho(r)$  is the DM mass density. In turn,  $\rho(r)$  is expressed here as a function of  $\mu(r)$  through the standard integral of the DM phase-space distribution function over the momentum

$$\rho(r) = \frac{g m}{2\pi^2 \hbar^3} \int_0^\infty dp p^2 f\left(\frac{p^2}{2m} - \mu(r)\right) , \quad (2.3)$$

where  $g$  is the number of internal degrees of freedom of the DM particle, with  $g = 1$  for Majorana fermions and  $g = 2$  for Dirac fermions. For definiteness, we will take  $g = 2$  in the sequel.

Another standard integral of the DM phase-space distribution function is the pressure

$$P(r) = \frac{1}{3\pi^2 m \hbar^3} \int_0^\infty dp p^4 f\left(\frac{p^2}{2m} - \mu(r)\right) \quad (2.4)$$

and from  $\rho(r)$  and  $P(r)$  other quantities of interest, such as the velocity dispersion  $\sigma(r)$  and the phase-space density  $Q(r)$  can be determined as

$$\sigma^2(r) = \frac{P(r)}{\rho(r)} , \quad Q(r) = \frac{\rho(r)}{\sigma^3(r)} . \quad (2.5)$$

We see that  $\mu(r)$  fully characterizes the fermionic DM halo in this Thomas–Fermi framework. The chemical potential is monotonically decreasing in  $r$  since eq. (2.2) implies

$$\frac{d\mu}{dr} = -\frac{G m M(r)}{r^2} , \quad M(r) = 4\pi \int_0^r dr' r'^2 \rho(r') . \quad (2.6)$$

Moreover, the fermionic DM mass density  $\rho$  is bounded at the origin due to the Pauli principle [9], and therefore the proper boundary condition at the origin is

$$\frac{d\mu}{dr}(0) = 0 . \quad (2.7)$$

Also notice from eq.(2.1) that, by assuming  $\phi(0) = 0$ , then  $\mu_0 \equiv \mu(0)$ , which plays the role of a Lagrange multiplier to be eventually eliminated in favor of  $\rho_0 \equiv \rho(0)$ , the mass density at the origin.

Eqs.(2.2) and (2.3) provide an ordinary nonlinear differential equation that determines selfconsistently the chemical potential  $\mu(r)$  and constitutes the Thomas–Fermi semi-classical approach. Fermionic DM in this approach has been previously considered in ref. [13].

In this semi-classical framework the stationary energy distribution function  $f(E)$  must be assigned beforehand. In a full-fledged treatment one would rather solve the cosmological DM evolution since decoupling till today, including the quantum dynamical effects which become important in the non-linear stage and close enough to the origin. Such a quantum dynamical calculation is beyond the scope of the present paper.

From eq.(2.4) and (2.5) we derive the local equation of state:

$$P(r) = \sigma^2(r) \rho(r) , \quad (2.8)$$

and the hydrostatic equilibrium equation

$$\frac{dP}{dr} + \rho(r) \frac{d\phi}{dr} = 0 . \quad (2.9)$$

The local equation of state eq.(2.8) generalizes the local perfect fluid equation of state for  $r$ -dependent velocity  $v(r)$ . As we see below, the perfect fluid equation of state is recovered both in the classical dilute limit and in the quantum degenerate limit.

Eliminating  $P(r)$  between eqs.(2.8) and (2.9) and integrating on  $r$  gives

$$\frac{\rho(r)}{\rho(0)} = \frac{\sigma^2(0)}{\sigma^2(r)} e^{-\int_0^r \frac{dr'}{\sigma^2(r')} \frac{d\phi}{dr'}} .$$

For constant  $v(r)$  this relation reduces to the baryotropic equation. Inserting this expression for  $\rho(r)$  in the Poisson's equation yields

$$\frac{d^2\phi}{dr^2} + \frac{2}{r} \frac{d\phi}{dr} = 4\pi G m \rho_0 \frac{\sigma^2(0)}{\sigma^2(r)} e^{-\int_0^r \frac{dr'}{\sigma^2(r')}} \frac{d\phi}{dr}.$$

This nonlinear equation generalizes the corresponding equation in the self-gravitating Boltzmann gas when  $\sigma^2(r)$  is constant.

We integrate the Thomas-Fermi nonlinear differential equations (2.2)-(2.3) from  $r = 0$  till the boundary  $r = R = R_{200} \sim R_{vir}$  defined as the radius where the mass density equals 200 times the mean DM density. It is useful to define dimensionless variables  $\xi$ ,  $\xi_R$ ,  $\nu(\xi)$  and the dimensionless one-parameter distribution function  $\Psi$  as

$$r = l_0 \xi \quad , \quad R = l_0 \xi_R \quad , \quad \mu(r) = E_0 \nu(\xi) \quad , \quad f(E) = \Psi\left(\frac{E}{E_0}\right) \quad , \quad (2.10)$$

where  $E_0$  is the characteristic one-particle energy of the DM halo and  $l_0$  is the characteristic length that emerges from the dynamical equations (2.2)-(2.3):

$$l_0 \equiv \frac{\hbar}{\sqrt{8G}} \left(\frac{9\pi}{m^8 \rho_0}\right)^{\frac{1}{6}} = R_0 \left(\frac{\text{keV}}{m}\right)^{\frac{4}{3}} \left(\rho_0 \frac{\text{pc}^3}{M_\odot}\right)^{-\frac{1}{6}} \quad , \quad R_0 = 18.709 \dots \text{ pc} \quad , \quad (2.11)$$

The self-consistent Thomas-Fermi equation (2.2)-(2.3) for  $\nu(\xi)$  takes the form

$$\frac{d^2\nu}{d\xi^2} + \frac{2}{\xi} \frac{d\nu}{d\xi} = -\frac{I_2(\nu)}{[I_2(\nu_0)]^{1/3}} \quad , \quad \rho(\xi_R) = 200 \bar{\rho}_{DM} \quad , \quad \nu'(0) = 0 \quad , \quad \nu_0 \equiv \nu(0) \quad , \quad (2.12)$$

where

$$I_n(\nu) \equiv (n+1) \int_0^\infty y^n dy \Psi(y^2 - \nu) \quad , \quad n = 1, 2, \dots \quad , \quad (2.13)$$

and we use the integration variable  $y \equiv p/\sqrt{2mE_0}$ .

We find the main physical galaxy magnitudes, such as the mass density  $\rho(r)$ , the average velocity of the particles  $v(r)$  and the pressure  $P(r)$  (which are all  $r$ -dependent) as:

$$\rho(r) = \rho_0 \frac{I_2(\nu(\xi))}{I_2(\nu_0)} \quad , \quad \sigma^2(r) = \sigma^2(0) \frac{I_2(\nu_0)}{I_4(\nu_0)} \frac{I_4(\nu(\xi))}{I_2(\nu(\xi))} \quad , \quad P(r) = P(0) \frac{I_4(\nu(\xi))}{I_4(\nu_0)} \quad , \quad (2.14)$$

$$\begin{aligned} \rho_0 &= \frac{m^4}{3\pi^2 \hbar^3} \left(\frac{2E_0}{m}\right)^{3/2} I_2(\nu_0) \quad , \quad P(0) = \frac{2E_0}{5m} \rho_0 \frac{I_4(\nu_0)}{I_2(\nu_0)} = \frac{\hbar^2}{5} \left(\frac{3\pi^2}{m^4}\right)^{\frac{2}{3}} \left[\frac{\rho_0}{I_2(\nu_0)}\right]^{5/3} I_4(\nu_0) \quad , \\ \sigma(0) &= V_0 \frac{[I_4(\nu_0)]^{1/2}}{[I_2(\nu_0)]^{5/6}} \left(\frac{\text{keV}}{m}\right)^{4/3} \left(\rho_0 \frac{\text{pc}^3}{M_\odot}\right)^{1/3} \quad , \quad V_0 = 2.751 \frac{\text{km}}{\text{s}} \quad . \end{aligned} \quad (2.15)$$

As a consequence, the total mass  $M_R$  enclosed in the sphere of radius  $R$  and the phase space density  $Q(r)$  turn to be

$$\begin{aligned} M_R &= 4\pi \int_0^R r^2 dr \rho(r) = 4\pi \frac{\rho_0 l_0^3}{I_2(\nu_0)} \int_0^{\xi_R} dx x^2 I_2(\nu(x)) = 4\pi \frac{\rho_0 l_0^3}{[I_2(\nu_0)]^{2/3}} \xi_R^2 |\nu'(\xi_R)| = \\ &= M_0 \frac{\xi_R^2 |\nu'(\xi_R)|}{[I_2(\nu_0)]^{2/3}} \left(\frac{\text{keV}}{m}\right)^4 \sqrt{\rho_0 \frac{\text{pc}^3}{M_\odot}} \quad , \quad M_0 = \frac{4\pi}{3} M_\odot \left(\frac{R_0}{\text{pc}}\right)^3 = 0.82296 \dots \times 10^5 M_\odot \quad , \end{aligned} \quad (2.16)$$

$$Q(r) = Q(0) \frac{I_2^{\frac{5}{2}}(\nu(\xi))}{I_4^{\frac{3}{2}}(\nu(\xi))} \frac{I_4^{\frac{3}{2}}(\nu_0)}{I_2^{\frac{3}{2}}(\nu_0)} \quad , \quad Q(0) = \frac{\sqrt{125}}{3\pi^2 \hbar^3} m^4 \frac{I_2^{\frac{5}{2}}(\nu_0)}{I_4^{\frac{3}{2}}(\nu_0)} \quad , \quad \nu_0 \equiv \nu(0) \quad , \quad \rho_0 = \rho(0) \quad . \quad (2.17)$$

We have systematically eliminated the energy scale  $E_0$  in terms of the central density  $\rho_0$ . [We may also choose the density at another point  $r \neq 0$ ]. Notice that  $Q(r)$  turns to be independent of  $E_0$  and therefore from  $\rho_0$ .



Besides the virial galaxy radius  $R = l_0 \xi_R$ , one can define the core size  $r_h$  of the halo by analogy with the Burkert density profile as

$$\frac{\rho(r_h)}{\rho_0} = \frac{1}{4} \quad , \quad r_h = l_0 \xi_h . \quad (2.18)$$

To explicitly solve eq. (2.12) we need to specify the distribution function  $\Psi(E/E_0)$ . But many important properties of the Thomas–Fermi semi-classical approximation do not depend on the detailed form of the distribution function  $\Psi(E/E_0)$ . Indeed, a generic feature of a physically sensible one-parameter form  $\Psi(E/E_0)$  is that it should describe degenerate fermions for  $E_0 \rightarrow 0$ . That is,  $\Psi(E/E_0)$  should behave as the step function  $\theta(-E)$  in such limit. In the opposite limit,  $\Psi(E/E_0)$  describes classical particles for  $\mu/E_0 \rightarrow -\infty$ . As an example of distribution function, we consider the Fermi–Dirac distribution

$$\Psi_{\text{FD}}(E/E_0) = \frac{1}{e^{E/E_0} + 1} . \quad (2.19)$$

The choice of  $\Psi_{\text{FD}}$  may be justified near the origin, where relaxation to thermal equilibrium is conceivable. Far from the origin however, the Fermi–Dirac distribution as its classical counterpart, the isothermal sphere, produces a mass density tail  $1/r^2$  that overestimates the observed tails of the galaxy mass densities. Notice indeed that the classical regime  $\mu/E_0 \rightarrow -\infty$  may be attained for large distances  $r$  since eq.(2.6) indicates that  $\mu(r)$  is always monotonically decreasing with  $r$ .

More precisely, large positive values of the chemical potential at the origin  $\nu_0 \gg 1$  correspond to the degenerate fermions limit which is the extreme quantum case and oppositely,  $\nu_0 \ll -1$  gives the diluted limit which is the classical limit. In this classical limit the Thomas-Fermi equations (2.2)-(2.3) become the equations for a self-gravitating Boltzmann gas.

We display in fig. 1 the density and velocity profiles. Namely, we plot  $\rho(r)/\rho_0$  and  $\sigma(r)/\sigma(0)$  as functions of  $r/R$  for  $\nu_0 \equiv \nu(0) = -5, 0, 5, 15, 25$  and in the degenerate fermion limit  $\nu_0 \rightarrow +\infty$ . The obtained fermion profiles are always cored. The sizes of the cores  $r_h$  defined by eq.(2.18) are in agreement with the observations, from the compact galaxies where  $r_h \sim 35$  pc till the spiral and elliptical galaxies where  $r_h \sim 0.2 - 60$  kpc. The larger and positive is  $\nu_0$ , the smaller is the core. The minimal core size arises in the degenerate case  $\nu_0 \rightarrow +\infty$  (compact dwarf galaxies).

Eqs.(2.14)-(2.16) cover the **full range** of physical galaxy situations from the quantum degenerate fermions (dwarf galaxies) until the dilute classical limit (spiral and elliptic galaxies) as we discuss in subsection II C. In addition, the galaxy length scale  $l_0$  and the galaxy mass  $M_R$  emerging from the Thomas-Fermi approach turn to be of the same order of magnitude of the Jeans' length and Jeans' mass, respectively which are here of semi-classical nature, containing  $\hbar$  and  $G$  [9].

#### A. Quantum degenerate limit: compact dwarf galaxies and minimal galaxy mass

The quantum degenerate limit is very instructive and we consider it now. In this limit  $\nu_0 \gg 1$ , the distribution function  $\Psi(E/E_0)$  becomes a step function  $\theta(-E)$  and all fermion states get filled till the Fermi level. Notice that the degenerate limit of the distribution function is **always** a step function  $\theta(-E)$  irrespective of the shape of the non-degenerate fermion distribution function  $\Psi(E/E_0)$ . Then, from eq.(2.13)

$$I_n(\nu)_{deg} = \nu^{\frac{n+1}{2}} , \quad (2.20)$$

The Thomas–Fermi equation (2.12) becomes

$$\frac{d^2\eta}{d\xi^2} + \frac{2}{\xi} \frac{d\eta}{d\xi} = -\eta^{3/2} , \quad \eta(\xi) \equiv \frac{\nu(\xi)}{\nu_0} , \quad \eta(0) = 1 , \quad \eta'(0) = 0 , \quad (2.21)$$

which we solve numerically for  $0 < \xi < \xi_R$  with  $\xi_R = 3.6537446 \dots$  the first zero of  $\eta(\xi)$  and the dimensionless core radius  $\xi_h = 2.269587 \dots$ . One then finds for the mass density and total mass in the degenerate limit

$$\begin{aligned} \rho_{deg}(r) &= \rho_0 \eta^{3/2}(\xi) = \frac{2^{3/2} m^{5/2}}{3 \pi^2 \hbar^3} \mu^{3/2}(r) \quad , \quad M_{deg,R} = 4 \pi \rho_0 l_0^3 \int_0^{\xi_R} d\tau \tau^2 \eta^{3/2}(\tau) = \\ &= \left( \hbar \sqrt{\frac{2\pi}{G}} \right)^3 \frac{\sqrt{\rho_0}}{(2m)^4} \xi_R^2 |\eta'(\xi_R)| = 2.714 \dots M_0 \left( \frac{\text{keV}}{m} \right)^4 \sqrt{\rho_0 \frac{\text{pc}^3}{M_\odot}} , \end{aligned}$$

$$M_{deg,h} = 1.856 \dots M_0 \left( \frac{\text{keV}}{m} \right)^4 \sqrt{\rho_0 \frac{\text{pc}^3}{M_\odot}}, \quad (2.22)$$

where the numerical result  $\xi_R^2 |\eta'(\xi_R)| = 2.71405512 \dots$  and  $\xi_h^2 |\eta'(\xi_h)| = 1.855893 \dots$  have been used and  $M_0$  is given by eq.(2.16). The density in the degenerate limit vanishes where  $\mu(r)$  does.

Finally, for the velocity dispersion we find from eqs. (2.14), (2.16) and (2.20)

$$\sigma_{deg}(r) = \sigma_{deg}(0) \eta^{1/2}(\xi) \quad , \quad \sigma_{deg}(0) = V_0 \left( \frac{\text{keV}}{m} \right)^{\frac{4}{3}} \left( \rho_0 \frac{\text{pc}^3}{M_\odot} \right)^{\frac{1}{3}}. \quad (2.23)$$

The phase-space density at the origin  $Q(0)$  takes in the degenerate limit its maximal value

$$Q_{deg}(0) = \frac{\rho_0}{\sigma^3(0)} = \frac{5\sqrt{5}}{3\pi^2} \frac{m^4}{\hbar^3} = 0.37760 \dots \frac{m^4}{\hbar^3}. \quad (2.24)$$

In the quantum degenerate limit  $\nu_0 \rightarrow +\infty$ , the DM fermions of the halo are in the minimally excited state, namely the (semiclassical) ground state for which the three basic quantities: halo radius, galaxy mass  $M_h$  and velocity dispersion, take their *minimum* values:

$$\begin{aligned} r_{h,min} &= 24.51 \dots \text{pc} \left( \frac{\text{keV}}{m} \right)^{\frac{4}{3}} \left( \rho_0 \frac{\text{pc}^3}{M_\odot} \right)^{\frac{1}{6}}, \quad \sigma_{min}(0) = 2.751 \frac{\text{km}}{\text{s}} \left( \frac{\text{keV}}{m} \right)^{\frac{4}{3}} \left( \rho_0 \frac{\text{pc}^3}{M_\odot} \right)^{\frac{1}{3}}, \\ M_{h,min} &= 2.9394 \dots 10^4 M_\odot \left( \frac{\text{keV}}{m} \right)^4 \sqrt{\rho_0 \frac{\text{pc}^3}{M_\odot}}. \end{aligned} \quad (2.25)$$

These minimum values are similar to the estimates for degenerate fermions eqs.(1.13), as it must be.

The masses of compact dwarf galaxies dominated by DM must be larger than the minimum mass  $M_{h,min}$  eq.(2.25). The lightest known galaxy of this kind is Willman I (see Table I). Imposing  $M_{h,min} < M_{Willman\ I} = 2.9 \cdot 10^4 M_\odot$  gives a minimal mass (a lower bound) for the WDM particle:

$$m > m_{min} = 1.91 \text{ keV}. \quad (2.26)$$

It must be stressed that these minimum physical values for degenerate WDM fermions eqs.(2.25)-(2.26) are independent of the WDM particle physics model. They are **universal** whatever is the shape of the distribution function  $f(E)$  in the non-degenerate regime.

As can be seen from eq.(2.25) the minimal value of the WDM particle mass  $m_{min}$  in eq.(2.26) is given by

$$m_{min} = 1.3094 \dots \text{keV} \left( \frac{10^4 M_\odot}{M^{lightest\ galaxy}} \right)^{\frac{1}{4}} \left( \frac{\rho_0^{lightest\ galaxy} \text{pc}^3}{M_\odot} \right)^{\frac{1}{8}}.$$

As a consequence, the error on  $m_{min}$  due to the observational error on the mass and central density of the lightest galaxy (Willman I, so far) is considerably reduced by the small exponents 1/4 and 1/8, respectively.

X-ray galaxy observations provide upper bounds for the particle mass for a specific WDM candidate: the sterile neutrino. If the sterile neutrinos are described by the Dodelson-Widrow (DW) model this upper bound turns to be [23]

$$m < 2.2 \text{ keV}. \quad (2.27)$$

Therefore, for WDM formed by DW sterile neutrinos their particle mass must be in the narrow interval  $1.91 \text{ keV} < m < 2.2 \text{ keV}$ .

More precise data for ultracompact dwarf galaxies as Willman I will make our bound eq.(2.26) more precise.

Improvements on our lower bound eq.(2.26) as well as on the upper bound eq.(2.27) from more precise galaxy data will lead to more stringent constraints on sterile neutrino WDM particle models.

### B. Classical dilute limit: large galaxies

In the classical dilute limit,  $\nu \ll -1$ , the FD distribution function eq.(2.19) becomes the Maxwell-Boltzmann distribution and we find from eqs.(2.12),

$$\Psi_{cl}(y^2 - \nu) = e^{\nu - y^2} \quad , \quad I_2^{cl}(\nu) = \frac{3}{4} \sqrt{\pi} e^\nu \quad , \quad I_4^{cl}(\nu) = \frac{15}{8} \sqrt{\pi} e^\nu \quad , \quad (2.28)$$

$$\begin{aligned} \frac{d^2 \nu}{d\xi^2} + \frac{2}{\xi} \frac{d\nu}{d\xi} &= - \left( \frac{3}{4} \sqrt{\pi} \right)^{\frac{2}{3}} e^\nu \quad , \quad \nu(0) = \nu_0 \quad , \quad \nu'(0) = 0 \quad , \\ Q_{cl}(r) &= \frac{1}{\sqrt{2} \pi^3} e^\nu \frac{m^4}{\hbar^3} \quad . \end{aligned} \quad (2.29)$$

In this limit from eq.(2.28), the ratio  $I_4^{cl}(\nu)/I_2^{cl}(\nu)$  becomes constant and the average velocity  $\sigma(r)$  from eqs.(2.14) becomes uniform. Furthermore, the numerical resolution of eq.(2.12) or eqs.(2.28) in the classical  $\nu_0 \ll -1$  regime yields

$$\begin{aligned} \xi_R &= 37.11 \dots e^{-\nu_0/3} \gg 1 \quad \text{and} \quad -\nu'(\xi_R) = 0.05318 \dots e^{\nu_0/3} \ll 1 \quad , \\ \xi_h &= 3.299 \dots e^{-\nu_0/3} \gg 1 \quad \text{and} \quad -\nu'(\xi_h) = 0.5578 \dots e^{\nu_0/3} \ll 1 \quad . \end{aligned} \quad (2.30)$$

Therefore, we see from eqs.(2.14), (2.16) that the size and mass for  $\nu_0 \ll -1$  and fixed  $\rho_0$  grow as

$$\begin{aligned} M_R &= 60.57 \dots e^{-\nu_0} M_0 \left( \frac{\text{keV}}{m} \right)^4 \sqrt{\rho_0 \frac{\text{pc}^3}{M_\odot}} \quad , \quad R = 694.3 \dots e^{-\nu_0/3} \left( \frac{\text{keV}}{m} \right)^{\frac{4}{3}} \left( \rho_0 \frac{\text{pc}^3}{M_\odot} \right)^{\frac{1}{6}} \text{ pc} \quad , \\ M_h &= 5.0202 \dots e^{-\nu_0} M_0 \left( \frac{\text{keV}}{m} \right)^4 \sqrt{\rho_0 \frac{\text{pc}^3}{M_\odot}} \quad , \quad r_h = 61.71 \dots e^{-\nu_0/3} \left( \frac{\text{keV}}{m} \right)^{\frac{4}{3}} \left( \rho_0 \frac{\text{pc}^3}{M_\odot} \right)^{\frac{1}{6}} \text{ pc} \quad . \end{aligned}$$

We see that in the classical regime,  $\nu_0 \rightarrow -\infty$ ,  $r_h$  and  $M_h$  can be arbitrarily large. Galaxies of any large mass can be obtained as solutions of the Thomas-Fermi equations (2.12).

### C. Physical galaxy properties from compact dwarf galaxies to large galaxies

The largest value for the phase space density corresponds to the quantum degenerate fermions limit while the smallest values appear in the classical dilute limit.

In the left panel of fig. 2 we plot from eq.(2.14) the dimensionless quantity

$$\frac{\hbar^3}{(\text{keV})^4} Q(0) = \frac{\sqrt{125}}{3 \pi^2} \frac{I_2^{\frac{5}{2}}(\nu_0)}{I_4^{\frac{3}{2}}(\nu_0)} \left( \frac{m}{\text{keV}} \right)^4 \quad . \quad (2.31)$$

In the right panel of fig. 2, we plot instead the dimensionless product

$$\frac{M_h}{M_\odot} \sqrt{\frac{1}{\rho_0} \frac{M_\odot}{\text{pc}^3}} = 0.82296 \dots 10^5 \frac{\xi_h^2}{I_2^{2/3}(\nu_0)} |\nu'(\xi_h)| \left( \frac{\text{keV}}{m} \right)^4 \quad , \quad (2.32)$$

where  $M_h$  is the halo mass, namely the galaxy mass inside the core radius  $r_h$  defined by eq.(2.18) and we used eqs.(2.14)-(2.16). In both cases we consider the two values  $m = 1$  and  $2$  keV and we put in the abscissa the product

$$r_h \left( \frac{\text{pc}^3}{M_\odot} \rho_0 \right)^{\frac{1}{6}} = R_0 \xi_h \left( \frac{\text{keV}}{m} \right)^{\frac{4}{3}} \quad \text{in parsecs} \quad , \quad (2.33)$$

where  $r_h = l_0 \xi_h$  is the core radius. The phase-space density  $Q(0)$  and the galaxy mass  $M_h$  are obtained by solving the Thomas-Fermi eqs.(2.12). We have also superimposed the observed values  $\hbar^3 Q_h / (\text{keV})^4$  and  $M_h \sqrt{M_\odot / [\rho_0 \text{ pc}^3]} (m/\text{keV})^4$  from Table I. Notice that the observed values  $Q_h$  from the stars' velocity dispersion are in fact upper bounds for the DM  $Q_h$ . This may explain why the theoretical Thomas-Fermi curves in the left

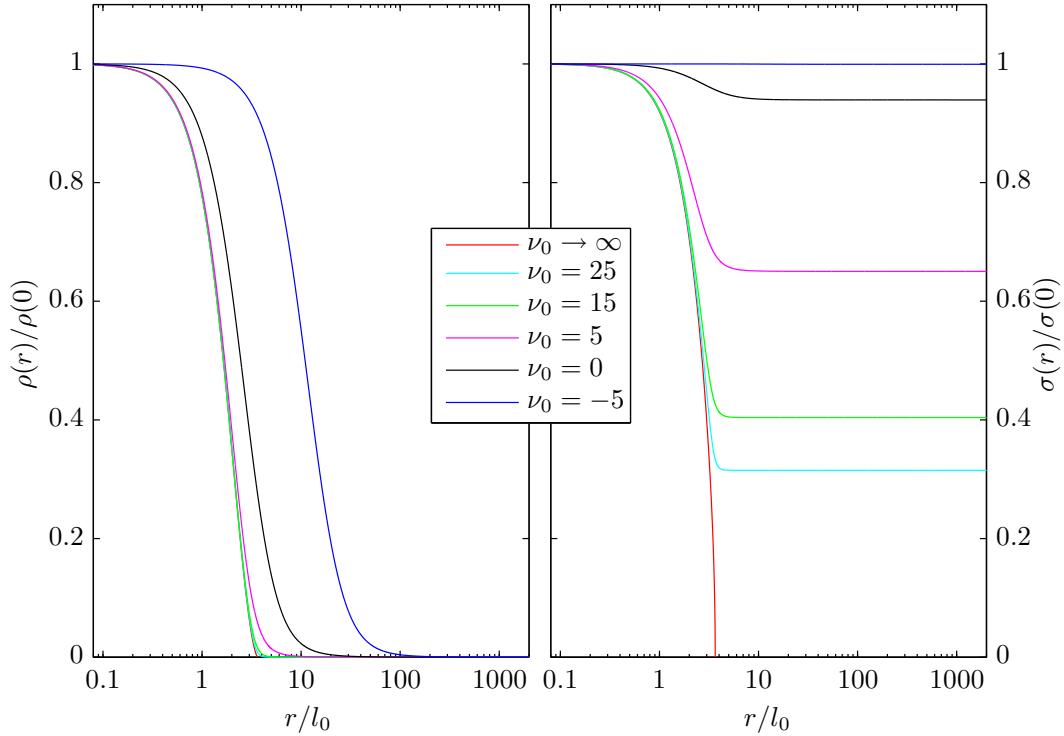


FIG. 1: Density and velocity profiles,  $\rho(r)/\rho_0$  and  $\sigma(r)/\sigma(0)$ , as functions of  $r/l_0$  for different values of the chemical potential at the origin  $\nu_0$ . Large positive values of  $\nu_0$  correspond to compact galaxies, negative values of  $\nu_0$  correspond to the classical regime describing spiral and elliptical galaxies. All density profiles are cored. The sizes of the cores  $r_h$  defined by eq.(2.18) are in agreement with the observations, from the compact galaxies where  $r_h \sim 35$  pc till the spiral and elliptical galaxies where  $r_h \sim .2 - 60$  kpc. The larger and positive is  $\nu_0$ , the smaller is the core. The minimal one arises in the degenerate case  $\nu_0 \rightarrow +\infty$  (compact dwarf galaxies).

pane of fig. 2 appear slightly below the observational data. Notice also that the error bars of the observational data are not reported here but they are at least about 10 – 20%.

The phase space density decreases from its maximum value for the compact dwarf galaxies corresponding to the limit of degenerate fermions till its smallest value for large galaxies, spirals and ellipticals, corresponding to the classical dilute regime. On the contrary, the halo radius  $r_h$  and the halo mass  $M_h$  monotonically increase from the quantum to the classical regime.

Thus, the whole range of values of the chemical potential at the origin  $\nu_0$  from the extreme quantum (degenerate) limit  $\nu_0 \gg 1$  to the classical (Boltzmann) dilute regime  $\nu_0 \ll -1$  yield all masses, sizes, phase space densities and velocities of galaxies from the ultra compact dwarfs till the larger spirals and elliptical in agreement with the observations (see Table I).

From figs. 2 we can extract important information on the fermion particle WDM mass.

We see from the left panel fig. 2 that decreasing the DM particle mass  $m$  moves the theoretical curves  $\hbar^3 Q(0)/(\text{keV})^4$  towards smaller  $Q(0)$  values and larger galaxy sizes, one over each other. In the right panel of fig. 2 we see that decreasing the DM particle mass  $m$  displaces the theoretical curves  $(M_h/M_\odot)\sqrt{M_\odot/[\rho_0 \text{ pc}^3]}$  towards larger galaxy masses and sizes, one over each other.

The small galaxy endpoint of the curves in figs. 2 corresponds to the degenerate fermion limit  $\nu_0 \rightarrow +\infty$  and its value depends on the WDM particle value  $m$ . For increasing  $m$ , the small galaxy endpoint moves towards smaller sizes while for decreasing  $m$ , it moves towards larger sizes.

We see from figs. 2 that decreasing the particle mass beyond a given value, namely for particle masses  $m \lesssim 1$  keV, the theoretical curves do not reach the more compact galaxy data. Therefore,  $m \lesssim 1$  keV is ruled out as WDM particle mass, in agreement with the bound eq.(2.26).

For growing  $m \gtrsim \text{keV}$  the left part of the theoretical curves corresponding to the lower galaxy masses and sizes, will not have observed galaxy counterpart. Namely, increasing  $m \gg \text{keV}$  would show an overabundance of small galaxies

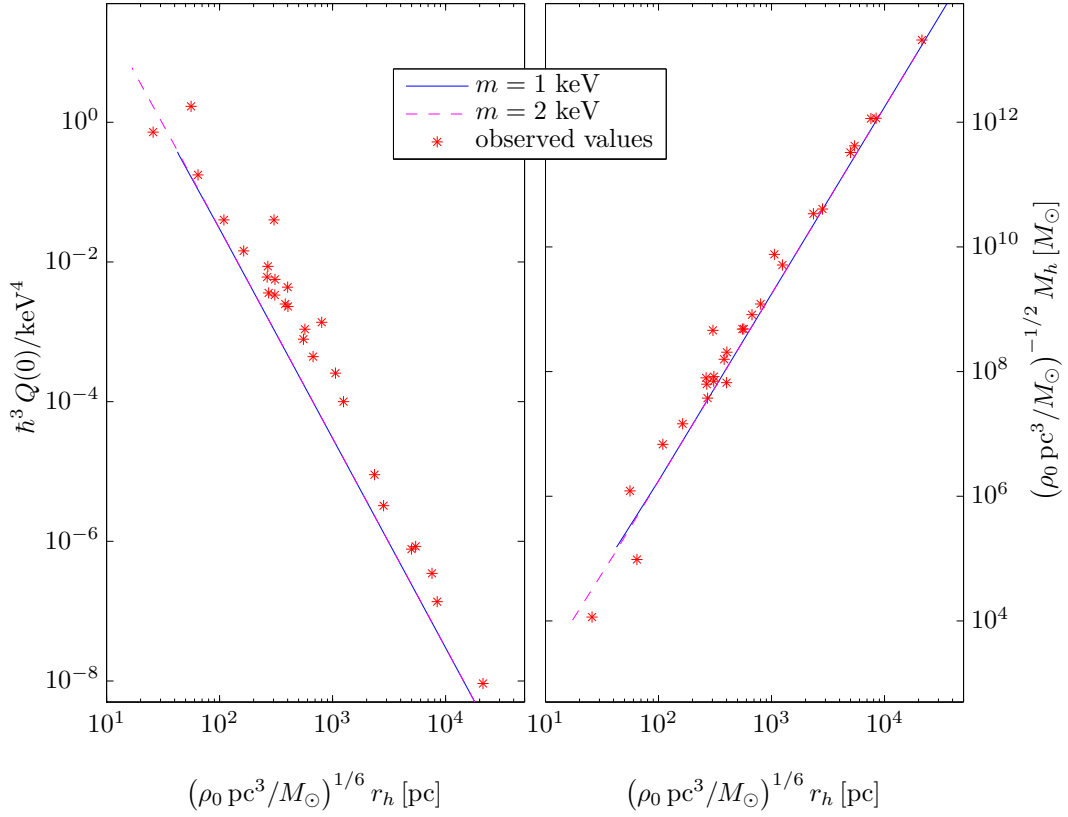


FIG. 2: In the left panel we display the galaxy phase-space density  $\hbar^3 Q(0)/(\text{keV})^4 = (m/\text{keV})^4 (\sqrt{125}/3 \pi^2) [I_2^{5/2}(\nu_0)/I_4^{3/2}(\nu_0)]$  defined in eq.(2.14) obtained from the numerical resolution of the Thomas-Fermi eqs.(2.12) for WDM fermions of mass  $m = 1$  and  $2 \text{ keV}$  versus the ordinary logarithm of the product  $\log_{10}\{r_h [\text{pc}^3 \rho_0/M_\odot]^{1/6}\} = \log_{10}[R_0 \xi_h (\text{keV}/m)^{4/3}]$  in parsecs. The red stars  $*$  are the observed values of  $\hbar^3 Q(0)/(\text{keV})^4$  from Table I. Notice that the observed values  $Q_h$  from the stars' velocity dispersion are in fact upper bounds for the DM  $Q_h$  and therefore the theoretical curve is slightly below them. In the right panel we display the galaxy mass  $(M/M_\odot) \sqrt{M_\odot/[\rho_0 \text{ pc}^3]} = 0.82296 \cdot 10^5 (\text{keV}/m)^4 \xi_h^2 |\nu'(\xi_h)|/I_2^{2/3}(\nu_0)$  obtained from the numerical resolution of the Thomas-Fermi eqs.(2.12) for WDM fermions of mass  $m = 1$  and  $2 \text{ keV}$  versus the product  $r_h [\text{pc}^3 \rho_0/M_\odot]^{1/6} = R_0 \xi_h (\text{keV}/m)^{4/3}$  in parsecs. The red stars  $*$  are the observed values of  $(M/M_\odot) \sqrt{M_\odot/[\rho_0 \text{ pc}^3]}$  from Table I. Notice that the error bars of the observational data are not reported here but they are at least about  $10 - 20\%$ .

(small scale structures) which do not have counterpart in the data. This is a further indication that the WDM particle mass is approximately around  $2 \text{ keV}$  in agreement with earlier estimations [10, 12].

In addition, the galaxy velocity dispersions from eq.(2.14)-(2.16) turn to be fully consistent with the galaxy observations in Table I.

The semiclassical Thomas-Fermi approach provides much stronger results than just the quantum bound on the phase-space density  $Q(r)$  only based on the Pauli principle,

$$Q(\vec{r}) \leq K \frac{m^4}{\hbar^3} \quad , \quad K = \mathcal{O}(1) \quad .$$

The primordial phase-space density  $Q$  fulfils this quantum bound [9]. Through classical time evolution,  $Q(\vec{r})$  in average ( $\bar{Q}$ ) will always fulfil this quantum bound since as it is known,  $\bar{Q}$  can only decrease with time. This quantum bound gives lower bounds in the galaxy core sizes in the range  $\sim 0.1 \text{ pc}$  [9] which are of the same order of magnitude as the core sizes obtained in the classical (non-quantum)  $N$ -body WDM simulations [15], which are unrealistically small cores compared with the observations. On the contrary, the Thomas-Fermi approach includes the quantum pressure and indeed succeeds to provide galaxy cores with the right sizes as shown in this paper.

To conclude, eqs.(2.14)-(2.16) indicate that the galaxy magnitudes: halo radius, galaxy masses and velocity dispersion obtained from the Thomas-Fermi quantum treatment for WDM fermion masses in the  $\text{keV}$  scale are fully

consistent with all the observations for all types of galaxies (see Table I). Namely, fermionic WDM treated quantum mechanically (as it must be) is able to reproduce the observed sizes of the DM cores of galaxies. These results strenght the discussion in sec. IB that compact galaxies are supported against gravity by the fermionic WDM quantum pressure.

It is highly remarkably that in the context of fermionic WDM, the simple stationary quantum description provided by the Thomas-Fermi approach is able to reproduce such broad variety of galaxies.

In addition, WDM simulations produce the right DM structures in agreement with observations for scales  $\gtrsim$  kpc [1].

### Acknowledgments

We are grateful to Peter Biermann for useful discussions in many occasions. We thank Daniel Boyanovsky and Paolo Salucci for useful remarks.

- 
- [1] P. Colín, O. Valenzuela, V. Avila-Reese, *Ap J*, 542, 622 (2000). J. Sommer-Larsen, A. Dolgov, *Ap J*, 551, 608 (2001). L. Gao and T. Theuns, *Science*, 317, 1527 (2007). A. V. Tikhonov et al., *MNRAS*, 399, 1611 (2009). J. Zavala et al., *Ap J*, 700, 1779 (2009). E. Papastergis et al., *Ap J*, 739, 38 (2011). M. R. Lovell et al., *MNRAS*, 420, 2318 (2012). D. Anderhalden et al. *arXiv:1212.2967*.
  - [2] R. F. G. Wyse, G. Gilmore, *IAU Symposium*, Vol. 244, p. 44-52 (2007), *arXiv:0708.1492*. J. van Eymeren et al. *A & A* 505, 1-20 (2009). W. J. G. de Blok, *Advances in Astronomy*, vol. 2010, pp. 1-15, *arXiv:0910.3538*. P. Salucci, Ch. Frigerio Martins, *arXiv:0902.1703*, *EAS Publications Series*, 36, 2009, 133-140.
  - [3] G. Gilmore et al., *Ap J*, 663, 948 (2007).
  - [4] M. Walker, J. Peñarrubia, *Ap. J.* 742, 20 (2011).
  - [5] R. P. Feynman, Lecture at the 1st. Conference on Physics and Computation, MIT 1981, *Int. J. Theor. Phys.* **21**,467(1982).
  - [6] V. Avila-Reese et al., *Ap J*, 559, 516 (2001). P. Colín, O. Valenzuela, V. Avila-Reese, *Ap J*, 673, 203 (2008). F. Villaescusa-Navarro and N. Dalal, *JCAP* 03, 024 (2011). J. Viñas, E. Salvador-Solé, A. Manrique, *MNRAS* 424, L6 (2012).
  - [7] R. B. Larson, *MNRAS*, 145, 405 (1969) and 147, 323 (1970). A. Lapi, A. Cavaliere, *Ap J*, 743, 127 (2011).
  - [8] C. Destri, H. J. de Vega, M. Lattanzi, N. G. Sanchez, in preparation.
  - [9] C. Destri, H. J. de Vega, N. G. Sanchez, *arXiv:1204.3090*, to appear in *New Astronomy*.
  - [10] H. J. de Vega, N. G. Sánchez, *Mon. Not. R. Astron. Soc.* **404**, 885 (2010) and *Int. J. Mod. Phys. A* **26**, 1057 (2011).
  - [11] P. Salucci et al., *MNRAS*, 378, 41 (2007).
  - [12] H. J. de Vega, P. Salucci, N. G. Sanchez, *arXiv:1004.1908*, *New Astronomy* **17**, 653 (2012), and references therein.
  - [13] F. Munyaneza, P. L. Biermann, *A & A*, 458, L9 (2006). N. Bilic, R. D. Viollier, *Phys. Lett. B* 408, 75 (1997) and *Eur. Phys. J. C* 11:173 (1999). P. H. Chavanis, *Phys. Rev.* **E65**, 056123 (2002), *Int. J. Mod. Phys. B* 20, 3113 (2006).
  - [14] M. Persic et al., *MNRAS*, 281, 27 (1996). S. H. Oh et al., *AJ*, 136, 2761 (2008). E. Memola et al., *A&A*, 534, A50 (2011).
  - [15] A. Macciò et al. *MNRAS* 424, 1105 (2012). S. Shao et al. *arXiv:1209*.
  - [16] J. D. Simon, M. Geha, *Ap J*, 670, 313 (2007) and references therein.
  - [17] J. D. Simon et al., *Ap. J.* 733, 46 (2011) and references therein.
  - [18] J. Wolf et al., *MNRAS*, 406, 1220 (2010) and references therein.
  - [19] J. P. Brodie et al., *AJ*, 142, 199 (2011). B. Willman and J. Strader, *AJ*, 144, 76 (2012).
  - [20] G. D. Martinez et al., *Ap J*, 738, 55 (2011).
  - [21] J. Woo et al. *MNRAS*, 390, 1453 (2008). N. F. Martin et al. *ApJ* 684, 1075 (2008).
  - [22] Matthew Walker, private communication.
  - [23] C. Watson, Z. Li, N. Polley, *arXiv:1111.4217*, *JCAP* 03, 18 (2012).